Polymer 50 (2009) 1025–1033

Contents lists available at ScienceDirect

Polymer

journal homepage: www.elsevier.com/locate/polymer

Liquid–liquid phase separation in a polyethylene blend monitored by crystallization kinetics and crystal-decorated phase morphologies

Shujun Wang [a], Changjiang Wu [b], Min-Qiao Ren [b], Ryan M. Van Horn [a], Matthew J. Graham [a], Charles C. Han [c], Erqiang Chen [b,*], Stephen Z.D. Cheng [a,*]

[a] College of Polymer Science and Polymer Engineering, Department of Polymer Science, The University of Akron, Akron, OH 44325-3909, USA
[b] Department of Polymer Science and Engineering, Peking University, Beijing, China
[c] Institute of Chemistry, Chinese Academy of Sciences, Beijing, China

ARTICLE INFO

Article history:
Received 14 October 2008
Received in revised form
30 November 2008
Accepted 4 December 2008
Available online 24 December 2008

Keywords:
Polyolefin blends
Liquid–liquid phase separation
Crystallization

ABSTRACT

A series of polyethylene (PE) blends consisting of a linear high density polyethylene (HDPE) and a linear low density polyethylene (LLDPE) with an octane-chain branch density of 120/1000 carbon was prepared at different concentrations. The two components of this set of blends possessed isorefractive indices, thus, making it difficult to detect their liquid–liquid phase separation *via* scattering techniques. Above the experimentally observed melting temperature of HDPE, $T_m = 133\,^{\circ}C$, this series of blends can be considered to be in the liquid state. The LLDPE crystallization temperature was below 50 °C; therefore, above 80 °C and below the melting temperature of HDPE, a series of crystalline–amorphous PE blends could be created. A specifically designed two-step isothermal experimental procedure was utilized to monitor the liquid–liquid phase separation of this set of blends. The first step was to quench the system from temperatures of known miscibility and isothermally anneal them at a temperature higher than the equilibrium melting temperature of the HDPE for the purpose of allowing the phase morphology to develop from liquid–liquid phase separation. The second step was to quench the system to a temperature at which the HDPE could rapidly crystallize. The time for developing 50% of the total crystallinity ($t_{1/2}$) was used to monitor the crystallization kinetics. Because phase separation results in HDPE-rich domains where the crystallization rates are increased, this technique provided an experimental measure to identify the binodal curve of the liquid–liquid phase separation for the system indicated by faster $t_{1/2}$. The annealing temperature in the first step that exhibits an onset of the decrease in $t_{1/2}$ is the temperature of the binodal point for that blend composition. In addition, the HDPE-rich domains crystallized to form spherulites which decorate the phase-separated morphology. Therefore, the crystal dispersion indicates whether the phase separation followed a nucleation-and-growth process or a spinodal decomposition process. These crystal-decorated morphologies enabled the spinodal curve to be experimentally determined for the first time in this set of blends.

1. Introduction

Single-site catalysts allow one to precisely control the structure of molecules including the incorporation of short-chain branches during synthesis of polyolefins [1–4]. The commercial success of polyolefins requires the use of binary blends to improve and optimize targeted properties [5–7]. It is common to blend two different polyethylenes (PE): a high density PE (HDPE) with zero or a low short-chain branch concentration that can crystallize and another linear low density PE (LLDPE) with high short-chain branch concentration that either crystallizes at much lower temperatures or that is a rubbery elastomer. The LLDPE increases the toughness and impact strength of the blend in the solid state as well as improves melt processability, while the HDPE enables the blend to maintain good tensile properties.

Even though the two components possess chemistries with the average elemental composition of CH_2, it is known that HDPE and LLDPE are not always miscible as a single phase. The miscibility of the two components is critically dependent on molecular characteristics such as molecular weight, short-chain branch concentration, branch type, composition, and processing conditions [8–18],

* Corresponding authors.
E-mail addresses: eqchen@pku.edu.cn (E. Chen), scheng@uakron.edu (S.Z.D. Cheng).

0032-3861/$ – see front matter © 2008 Elsevier Ltd. All rights reserved.
doi:10.1016/j.polymer.2008.12.028

although some of the results reported in those studies are still being debated. Most PE blends exhibit an upper critical solution temperature (UCST) [19]. Since at least one component is crystallizable, there is an interplay between phase separation and crystallization.

One recent investigation into the interplay of liquid–liquid phase separation and crystallization in a PE blend involved PE components that had hexane and butane branches at different compositions [20–22]. In the hexane-branched PE, the branch concentration was 9 per 1000 carbon atoms with a molecular weight of 112 kg/mol, while the butane-branched PE had a branch concentration of 77 per 1000 carbon atoms with a molecular weight of 77 kg/mol. The hexane-branched PE crystallized at much high temperatures than the butane-branched PE. Using scattering and optical microscopy techniques, a UCST phase diagram was obtained. The binodal curve and its intersection with the melting temperature depression curve of the hexane-branched PE crystals were also experimentally determined [20]. Within the phase-separated region, the extrapolated melting temperatures were found to be invariant with respect to concentration. This implies that the crystallization started after the concentration evolution of the liquid–liquid phase separation process was complete.

The main difficulty in studying this type of PE blend lies in how to precisely identify and measure separately the crystallization and liquid–liquid phase separation kinetics. In the same series of PE blends described above at a 50/50 composition, the crystal growth rates were measured after quenching the samples from the homogeneous melt to different crystallization temperatures using polarized light microscopy (PLM). The growth rates of the liquid–liquid phase separation in the coarsening stage were monitored utilizing a small-angle light scattering technique [21]. It was found that a kinetic cross-over temperature for the phase separation and crystallization rates takes place at 118 °C. When the crystallization temperature is below 118 °C, the crystallization rate was faster than the phase separation rate, and so, crystallization dominated the final phase morphology. Significantly above this temperature, the phase separation process dominated the final phase morphology. Near 118 °C, the two processes competed with each other.

The earliest recognition of the inter-dependence between liquid–liquid phase separation and crystallization in polymer blends was reported more than 20 years ago [23,24]. Since then, a number of different crystalline–amorphous polymer blend systems have been investigated. Since the equilibrium crystalline and morphological states are never reached in experimental time scales in polymer blends, the interplay of these two processes is obscured by the appearance of metastable states. Therefore, we need to take these temperature and time dependent metastable states into account [25–27].

Our interest is in monitoring the liquid–liquid phase separation in a crystalline–amorphous blend *via* crystallization kinetics and phase morphology. An experimental procedure was specifically designed such that liquid–liquid phase separation occurs before crystallization. This experimental procedure is a two-step isothermal process. The first step is to isothermally anneal the blend to reach concentration equilibrium at temperatures below the binodal curve boundary yet above the melting temperature of the crystalline phase to prevent crystallization. This leaves the phase morphology in a metastable state [27]. In the second step, the sample is isothermally crystallized by quenching it to a lower temperature where crystallization occurs rapidly. Further concentration changes in the phase domains are minimal because of the rate of crystallization. Additionally, the phase morphology of the domains is illuminated by crystal decoration.

In order to test this experimental approach, a series of PE blends were made. They consisted of an HDPE component and an LLDPE component that possessed randomly distributed octane branches at a concentration of 120 branches per 1000 carbon atoms. Utilizing the two-step isothermal process described above, both the crystallization kinetics and the phase morphology of these binary blends were observed to determine the binodal and spinodal curves of the liquid–liquid phase separation.

2. Experimental section

2.1. Materials and sample preparation

A series of PE blends was prepared. One of the components in the series of blends was an HDPE with a weight average molecular weight of 80 kg/mol. Another component was an LLDPE with randomly distributed octane branches with a weight average molecular weight of 70 kg/mol and an octane branch concentration of 120 per 1000 carbon atoms. The components have polydispersities of ~2. The HDPE is the crystalline component of this series, and the LLDPE is the amorphous component above 80 °C. In order to intimately mix these blends, both components were dissolved in xylene at 120 °C for 24 h. The solution was then quickly poured into a large excess amount of chilled methanol, and the blends rapidly precipitated. After filtration, the blend samples were washed with methanol and dried in a vacuum oven for 3 days. The samples were then quenched in liquid nitrogen and became powders.

For differential scanning calorimetry (DSC) experiments, the sample weight was about 1.0 mg, and the pan weights were kept constant at a precision of ±0.001 mg. Each sample was only used once. This is because after the samples are phase-separated and crystallized, intimate mixing of both components back to a single-phase blend takes too long to occur [28,29]. The samples used for morphological observations in PLM, phase contrast optical microscopy (PCOM) and atomic force microscopy (AFM) were prepared from the blend samples as described above and melted at 190 °C between two glass slides. These glass slides were then pressed to form films. The film thickness was controlled to be about 5 μm.

2.2. Equipment and experiments

The two-step isothermal method was conducted on a series of different blend compositions using a Perkin–Elmer PYRIS Diamond DSC with an Intracooler 2P apparatus. The temperatures and heat flows were calibrated using material standards at a cooling and heating rate of 10 °C/min. The sample was heated to 190 °C for 10 min to eliminate the thermal history and then quenched to the prescribed annealing temperature which ranged between 190 °C and 150 °C at intervals of 5 °C. At each temperature, the system was isothermally annealed for at least 6 h to allow any liquid–liquid phase separation to reach the late stage of coarsening and then quickly quenched to a lower preset temperature (such as at 120 °C) to crystallize the HDPE component. The preset temperature changed with the HDPE concentration to keep the overall crystallization kinetics in a convenient range for DSC analysis. Heat flow versus crystallization time was recorded by the DSC. The crystallization kinetics were characterized by the crystallization half-time ($t_{1/2}$), as defined by the time where 50% of the final crystallinity has been achieved. The crystallinity of each sample was measured by subsequent heating at 10 °C/min after the second-step isothermal crystallization without further cooling to room temperature and compared to the equilibrium heat of fusion of PE (293 J/g) [30].

Phase morphologies after annealing and crystallization with the two-step isothermal method were observed with PLM and PCOM (Olympus BH-2). Both of them were coupled with a calibrated

Mettler heating stage (FP-90). An AFM (Digital Instrument Nanoscope IIIA) in tapping mode was utilized to obtain a modulus map and surface topology map of the blends. The modulus map is derived from AFM phase information and goes beyond providing simple topographical information to show variations in surface modulus which can be associated with compositional variations in the different phase domains. All AFM images were measured at a temperature of 80 °C, which is higher than the melting temperature of LLDPE but lower than the melting temperature of HDPE. This enabled the modulus map to differentiate between the HDPE-rich phase and the LLDPE-rich phase. The scanner was calibrated in both lateral and vertical directions using a standard grid. A typical measurement was a scan size of 40 μm, a scan rate of 0.5 Hz with operation and resonance frequencies of 300 kHz, and a resolution of 512 × 512.

3. Results and discussion

3.1. Overall crystallization rates of the blends and determination of the binodal curve for liquid–liquid phase separation

Fig. 1a shows a set of overall crystallization heat flow thermal diagrams at 120 °C recorded by DSC for a 25/75 HDPE/LLDPE blend. Note that since each sample was only used once, the heat of crystallization shown in this figure cannot be compared to each other directly to obtain information about the crystallinity difference. Each thermal diagram corresponds to a different first-step annealing temperature ranging from 175 °C to 140 °C at a 5 °C interval. Since all of these annealing temperatures are above the melting temperatures of both PE components of the blend, no crystallization occurs during the annealing. When the first-step annealing temperature is below the binodal curve, liquid–liquid phase separation occurs. In a UCST system quenched below the binodal curve, the composition of the two phases is fixed by the tie-line intersection with the binodal curve, and the weight fraction of each phase is determined by the initial blend concentrations as well as the final phase concentrations at each temperature according to the lever rule [27]. In the 25/75 HDPE/LLDPE blend, the phase separation results in a dispersed HDPE-rich phase in an HDPE-poor matrix. After quenching the system further to crystallize the HDPE component and the LLDPE component remains a liquid, the effect of the liquid–liquid phase separation on the HDPE crystallization kinetics can be identified. It is expected that the change in the crystallization rate after the liquid–liquid phase separation occurs in the isothermal annealing. This is because within the HDPE-rich domains the probability of HDPE adsorbing onto the crystal growth front and crystallizing is higher than that in the miscible blend. This can be categorized into the so-called "poisoning" effects [27] which in the past described either polymer blends with identical chemical structure but different molecular weights [31–33] or with different chemical structures, one crystalline and one amorphous, but miscibility in the melt [34–36]. In the current case, the blends possess the identical average elemental composition of CH_2 but have different molecular architectures. A decrease in $t_{1/2}$ is, therefore, an indication of liquid–liquid phase separation, and the onset of this decrease indicates the temperature on the binodal curve at which the liquid–liquid phase separation occurs.

Fig. 1b is a plot of the $t_{1/2}$ values of the overall crystallization at 120 °C versus the annealing temperature. As we can see in this figure, the $t_{1/2}$ values remain constant when the annealing temperature is above 170 °C. Below this temperature, the $t_{1/2}$ values start to decrease. If the isothermal crystallization peak time (t_p) in Fig. 1a is used to characterize the overall crystallization kinetics instead of $t_{1/2}$, identical results are observed. The independence of $t_{1/2}$ with respect to the annealing temperature above 170 °C in the first step indicates that HDPE and LLDPE are miscible. The decrease

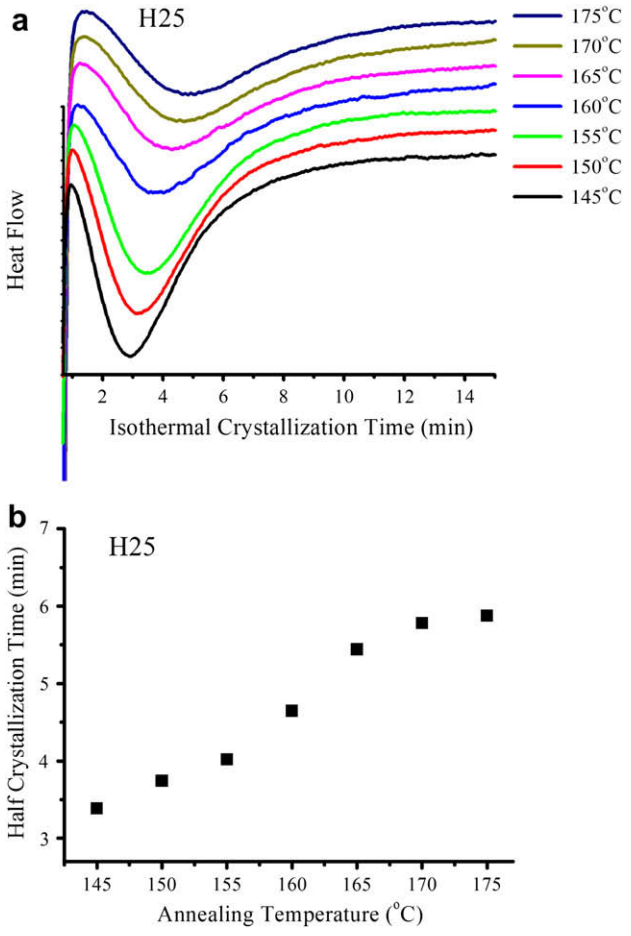

Fig. 1. (a) Set of DSC isothermal crystallization thermal diagrams at 120 °C for a blend of 25/75 HDPE/LLDPE after annealing at different temperatures for 6 h in the first step of the two-step isothermal experiment. (b) Relationship between the crystallization $t_{1/2}$ values deduced from the DSC results in (a) versus annealing temperatures in the first step for a blend of 25/75 HDPE/LLDPE. The onset temperature where the overall crystallization rate increases (the $t_{1/2}$ value decreases) is at 170 °C.

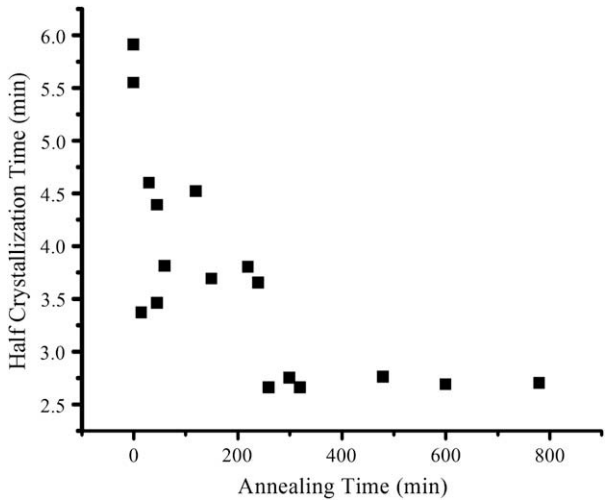

Fig. 2. The $t_{1/2}$ values of the overall crystallization at 124 °C versus annealing times at 150 °C for a blend of 45/55 HDPE/LLDPE.

in the $t_{1/2}$ values with decreasing annealing temperature indicates that 170 °C is the threshold below which the HDPE/LLDPE blend is phase separated. In Fig. 1b, at temperatures far below 170 °C, the HDPE-rich phase has an even higher HDPE concentration due to deeper quenching below the binodal curve, and thus, the crystallization rate is increasingly faster. The $t_{1/2}$ values for overall crystallization decrease as the HDPE concentration in the dispersed phase increases.

As the phase weight fractions develop in the early stage of phase separation, the overall crystallization rate will be annealing time dependent. In the late stage of phase separation, when the equilibrium phase weight fraction is reached, the overall crystallization rate should be constant. Note that even when the overall crystallization rate becomes constant, this only indicates that the phase-separated blend reaches the equilibrium weight fractions. However, the phase morphology of the liquid–liquid phase separation of the blend is still in a metastable state [26,27]. Furthermore, in these phase-separated morphologies, the HDPE-rich domains possess sizes which must be large enough (usually in the micrometer scale) to not affect the crystallization rates [37].

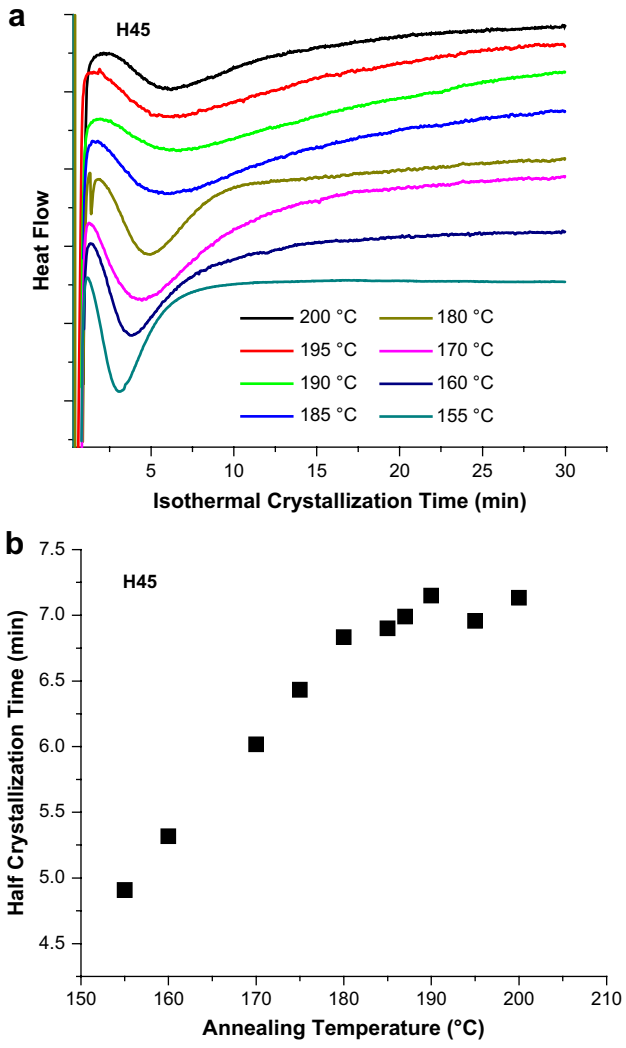

Fig. 3. (a) Set of DSC isothermal crystallization thermal diagrams at 122 °C for a blend of 45/55 HDPE/LLDPE after annealing at different temperatures for 6 h in the first step of the two-step isothermal experiment. (b) Relationship between the crystallization $t_{1/2}$ values deduced from the DSC results in (a) versus annealing temperatures in the first step for a blend of 45/55 HDPE/LLDPE. The onset temperature where the overall crystallization rate increases (the $t_{1/2}$ value decreases) is at 185 °C.

Fig. 2 demonstrates this principle for a blend with a 45/55 HDPE/LLDPE composition, which is close to the critical composition (see below). The isothermal annealing temperature in the first step was set at 150 °C, and the blend samples were maintained at that temperature for different annealing times. The samples were then quenched to a crystallization temperature of 124 °C to allow the HDPE to crystallize. It is evident from this figure that the annealing time at 150 °C must be longer than 300 min in order to reach a constant overall crystallization rate. The length of time needed reflects the slow liquid–liquid phase separation kinetics to reach the equilibrium phase weight fractions with sufficiently large domain sizes. For the rest of the paper, including blends at other concentrations, the annealing time was longer than 300 min to ensure a constant overall crystallization rate and that changes in

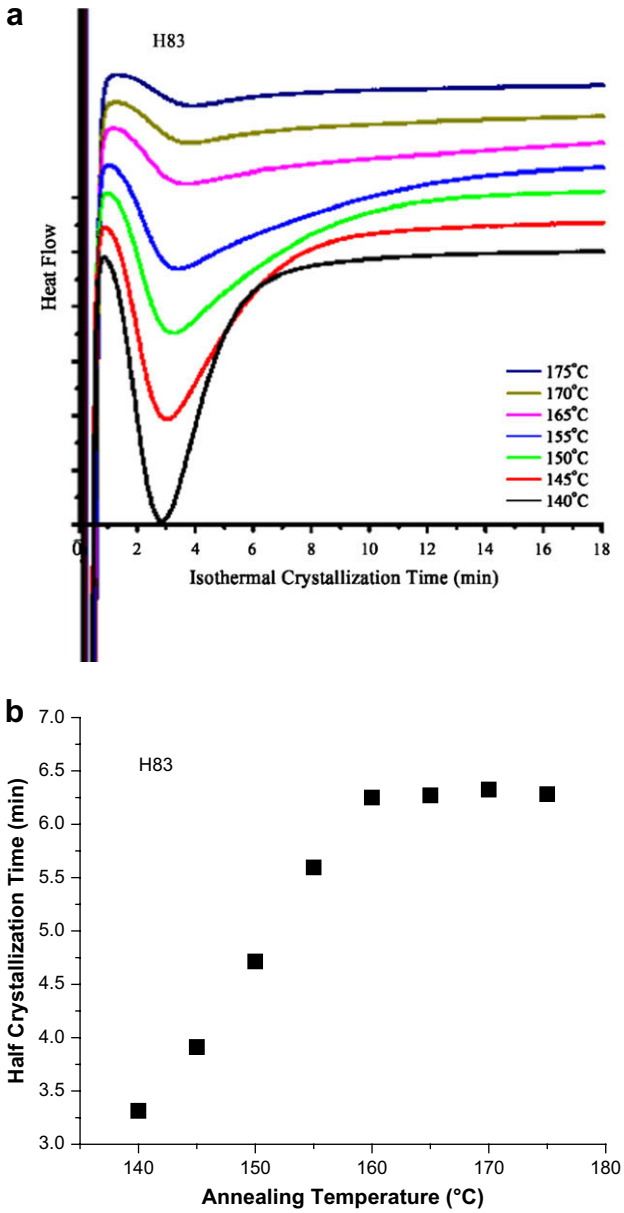

Fig. 4. (a) Set of DSC isothermal crystallization thermal diagrams for a blend of 83/17 HDPE/LLDPE after the samples were isothermally annealed at different temperatures in the first step for 6 h. (b) Relationship between the $t_{1/2}$ values of overall crystallization in (a) and annealing temperature for a blend of 83/17 HDPE/LLDPE. The overall crystallization rate increases (the $t_{1/2}$ value decreases) at 160 °C.

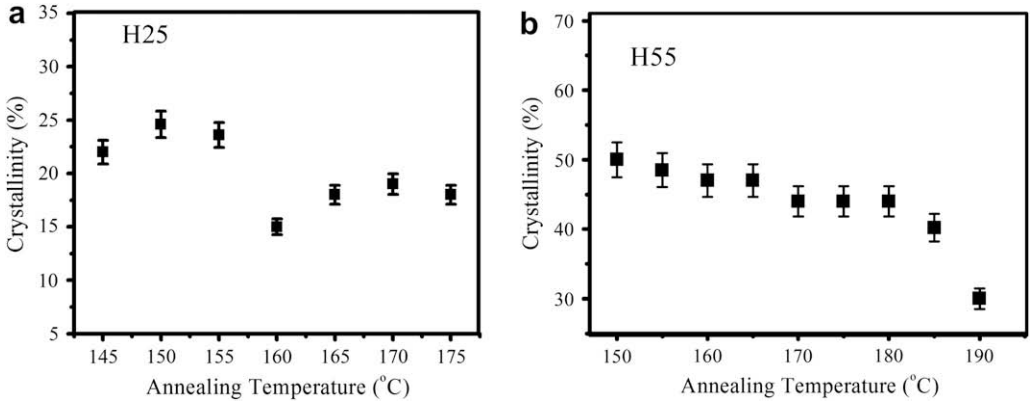

Fig. 5. HDPE crystallinity changes as a function of annealing temperature in the first step for two blends: (a) 25/75 after crystallization at 120 °C and (b) 55/45 HDPE/LLDPE after crystallization at 122 °C.

the $t_{1/2}$ value in these experiments were solely indications of reaching the binodal curve.

Since the two components have a comparable magnitude of molecular weight (around 10^5 g/mol), the critical composition is around 50/50 HDPE/LLDPE. Fig. 3a shows a set of DSC isothermal diagrams of the crystallization process at 122 °C for a 45/55 HDPE/LLDPE blend after the samples were annealed at different temperatures for 6 h. It is evident that the onset annealing temperature shifts to a much higher temperature of 185 °C as compared to the other blend compositions. This can be clearly observed in Fig. 3b in which the $t_{1/2}$ versus annealing temperatures is plotted.

When HDPE was the major component, such as in the case of 83/17 HDPE/LLDPE, the liquid–liquid phase separation consisted of a dispersed LLDPE-rich phase and an HDPE-rich matrix phase. Fig. 4a shows the experimentally observed DSC thermal diagrams for the overall crystallization at 124 °C, and Fig. 4b is a plot of $t_{1/2}$ versus annealing temperature. Again, since each sample was only used once, the heat of crystallizations shown in this figure cannot be compared to each other directly to obtain information about the crystallinity difference. It is evident that the crystallization rate increases after liquid–liquid phase separation even when HDPE is the majority phase.

Comparing Fig. 4a with Fig. 1a, the isothermal crystallization DSC thermal diagrams of the 83/17 HDPE/LLDPE blend exhibit different behaviors after phase separation. For the 25/75 HDPE/LLDPE blend, the most apparent change is that the t_p of crystallization is shifted as shown in Fig. 1a, yet the shape of the curve and the heat of crystallization do not alter. However, in the 83/17 HDPE/LLDPE blend, the overall crystallization t_p values are less shifted, but the shape of the diagrams before and after t_p has noticeably changed as shown in Fig. 4a. Curves are shallower at the higher annealing temperatures when the crystallization takes place in the miscible blend and steeper at the lower annealing temperatures after the phase separation has occurred. As a result, the crystallization $t_{1/2}$ values change drastically as shown in Fig. 4b. In this case, the t_p and $t_{1/2}$ values do not closely correspond to each other. This shape change as shown in Fig. 4b is due to the fact that when the crystallization takes place in the miscible blend, the HDPE crystallizes out of the miscible liquid and leaves an increasingly larger amount of LLDPE. Therefore, the concentration of the HDPE is continuously decreasing, leading to a prolonged crystallization process.

Furthermore, the crystallinity is dependent on the annealing temperature in the first step. It was found that when the crystallization rate starts increasing there is also a change in crystallinity. Fig. 5 shows the crystallinities for the two blends with HDPE concentrations of 25% and 55% measured during heating after the second-step isothermal crystallization at 120 °C and 122 °C, respectively. The crystallinities in this figure have been normalized by taking the weight fraction of HDPE into account. At the onset temperature of phase separation, the crystallinities discontinuously increase when the annealing temperature enters into the liquid–liquid phase separation region. This observation indicates that liquid–liquid phase separation not only enhances the overall crystallization kinetics, but also increases the quality and/or quantity of the crystals in the blend.

For all blends with HDPE concentrations between 15% and 83%, trends similar to those shown in Figs. 1–4 are observed. Using blends with different compositions, the binodal curve across the entire composition range can be constructed. The closed squares in Fig. 6 are the onset temperatures of the $t_{1/2}$ value changes for each of the HDPE concentrations obtained in this series of HDPE/LLDPE blends. The result is a binodal-like curve for liquid–liquid phase separation in terms of phase stability that should be close to the thermodynamic binodal curve of the liquid–liquid phase separation. It is evident that this binodal curve is more or less symmetric with the critical point at an HDPE concentration of 48%. The critical temperature is at 187 °C. The symmetric shape is evidence of the comparable molecular weights used in this series of blends.

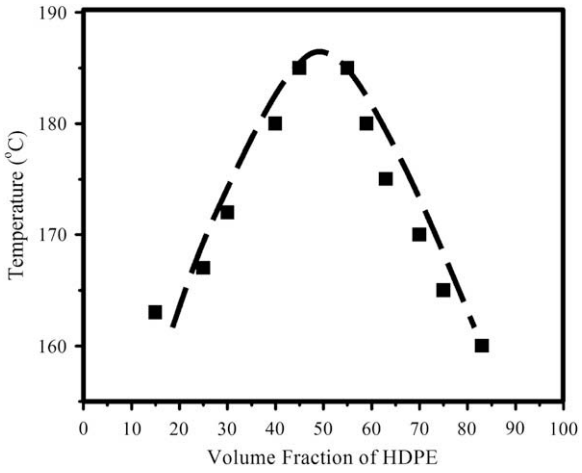

Fig. 6. Binodal curve for the HDPE/LLDPE blend at varying compositions deduced from the onset temperatures where the $t_{1/2}$ value starts to decrease (the overall crystallization rate starts to increase).

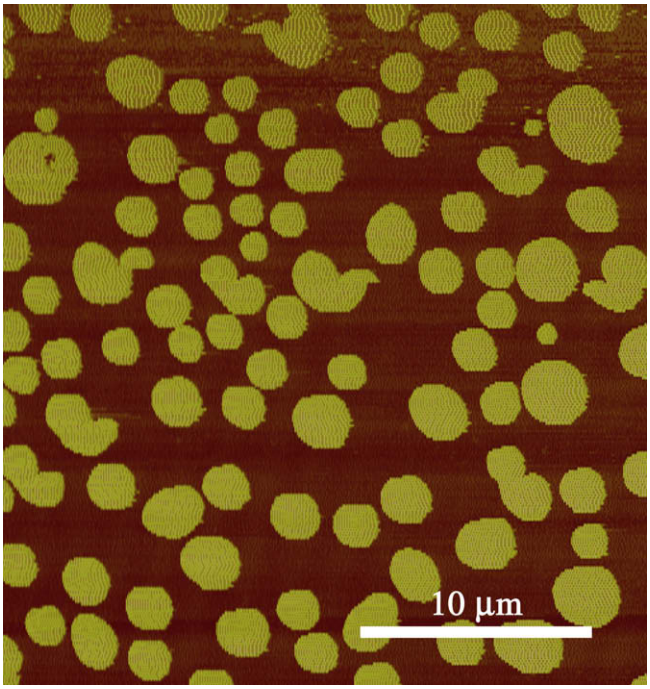

Fig. 7. AFM image of a blend of 40/60 HDPE/LLDPE crystallized at 123 °C after annealing at 175 °C for 24 h. The nucleation-limited mechanism with spherical phase morphology can be observed, indicating that the phase separation occurs in between the binodal and spinodal curves.

3.2. Crystal-decorated phase morphologies of the blends and the determination of the spinodal curve for the liquid–liquid phase separation

The spinodal curve in liquid–liquid phase separation is often difficult to determine experimentally for crystalline–amorphous blends when the two components have isorefractive indices, so their spinodal curves in the phase diagrams are typically based on theoretical calculations. In this study, we try to utilize both crystallization and liquid–liquid phase separation to construct a spinodal curve *via* morphological observations.

When the annealing temperature is in the metastable region between the binodal and spinodal curves, phase separation occurs through a nucleation-and-growth mechanism resulting in droplet-like domains by overcoming a nucleation barrier. When the annealing temperature is in the unstable region (below the spinodal curve), liquid–liquid phase separation follows a spinodal decomposition mechanism, and the phases form bicontinuous domains without any energy barrier [27,38–40]. As long as it is metastable, or does not reach the two-layer equilibrium morphology (which can never be reached), one can use the resultant phase morphology to distinguish between these two mechanisms [27].

Fig. 7 is an AFM phase image of an HDPE/LLDPE 40/60 blend crystallized at 123 °C after the sample was annealed at 175 °C for 24 h. As shown in Fig. 6, this annealing temperature is below the binodal curve as determined by the crystallization kinetics study. Droplet domains with diameters ranging from 1 to 4 μm can be clearly observed. Furthermore, this phase image indicates that within the droplets, the materials' modulus is higher than the matrix. This reveals that within the droplets the major component, HDPE, has become a crystalline-solid; while, the matrix is still a liquid within which the amorphous LLDPE is the major component. Based on this phase morphology observation, it can be concluded that the phase separation that takes place while annealing at 175 °C is between the binodal and spinodal curves corresponding to the nucleation-and-growth mechanism. This type of droplet morphology can be observed up to an annealing temperature of 180 °C, which coincides with the experimentally determined binodal curve.

Fig. 8a shows a PCOM image of the same sample after it was annealed at 170 °C for 24 h and then quenched to 123 °C to crystallize the HDPE. This figure shows crystalline spherulites impinging on each other in a bicontinuous phase morphology on a large length scale. Fig. 8b is a PLM image of Fig. 8a at the same location. It is evident from the crystalline spherulite decoration in the HDPE-rich domains that the phase morphology is bicontinuous. This indicates that the phase separation mechanism was spinodal decomposition, and therefore, the annealing temperature was below the spinodal line.

The AFM image in Fig. 9a was taken for an identical blend after annealing at 145 °C for 24 h and crystallizing at 123 °C. As in Fig. 8, this figure also shows a bicontinuous phase morphology with a number of crystals in the HDPE-rich domains. Fig. 9b is the

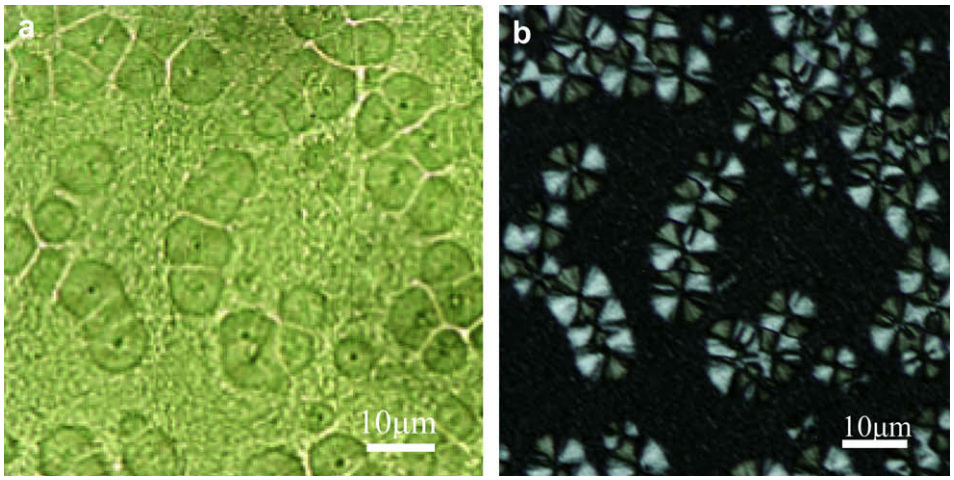

Fig. 8. Phase contrast microscopy (PCOM) (a) and PLM (b) images of a blend of 40/60 HDPE/LLDPE crystallized at 123 °C after isothermal annealing at 170 °C for 24 h. (a) The spinodal decomposition mechanism bicontinuous phase morphology, indicating that the phase separation occurs below the spinodal curve; (b) the HDPE spherulites grow within the bicontinuous phase domains.

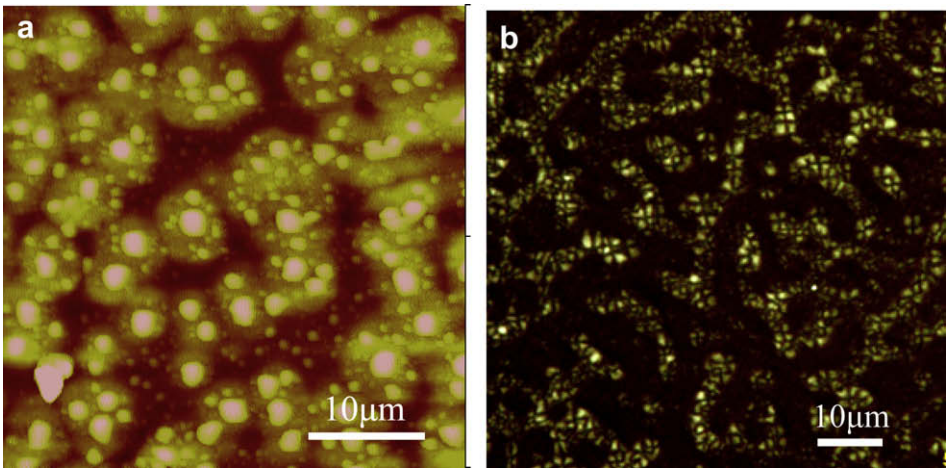

Fig. 9. AFM (a) and PLM (b) images of a blend of 40/60 HDPE/LLDPE crystallized at 123 °C after isothermal annealing at 145 °C for 24 h.

corresponding PLM image that shows a number of crystalline spherulites formed in the HDPE-rich domains. Compared with Fig. 8b, the bicontinuous domains are smaller in Fig. 9b, indicating that the increased viscosity at the lower annealing temperature has increased the coarsening time of the phase morphology. It may also be due in part to the change in dominant (Cahn–Hilliard) wavelength with quenching depth. However, despite the difference in size, these phase separation morphologies are self-similar.

For blends with HDPE as the major component, crystallization occurs in the matrix. Fig. 10a shows an AFM image for a 70/30 HDPE/LLDPE blend crystallized at 120 °C after annealing at 170 °C for 24 h. It is evident that the non-crystallizable LLDPE-rich droplets at 100 °C are the minority phase, and the HDPE-rich phase is now the crystallized spherulitic matrix. Fig. 10b is the corresponding PLM image. This phase morphology indicates that the liquid–liquid phase separation occurs through the nucleation-and-growth mechanism.

On the other hand, Fig. 11 is the PLM image for the same blend crystallized at 120 °C after annealing at 155 °C for 24 h in the first step. The bicontinuous phase morphology indicates that the spinodal decomposition mechanism was dominant. The only difference between Figs. 7 and 8 and Figs. 10 and 11 is that the minority and majority phase compositions in the latter figures are inversed.

It is evident that even after a prolonged annealing time of 24 h, the coarsening of the bicontinuous phase domains as observed in Figs. 8, 9 and 11 does not lead to a change of the phase morphology. Liquid–liquid phase separation morphology changes can thus be used to experimentally identify the mechanism of the phase separation. Using this approach at different compositions, the spinodal line in the phase stability diagram can be experimentally determined. A complete phase diagram with the experimentally determined binodal and spinodal curves is shown in Fig. 12. The open circles in this figure are obtained based on the observations where the phase morphology is changed to become the bicontinuous phase separation being decorated by the spherulitic crystal morphology.

One issue that remains is whether during the quench to the crystallization temperature, a further phase separation occurs and whether this could obscure the observations. We have estimated that the overall crystallization rate at the crystallization temperature in our experiment is about twenty times faster than the liquid–liquid phase separation rate. Therefore, further phase separation to obscure the already coarsened phase morphology is limited and hindered by the crystallization.

Based on the experimentally observed binodal curve, the spinodal line can also be calculated theoretically using Flory–Huggins

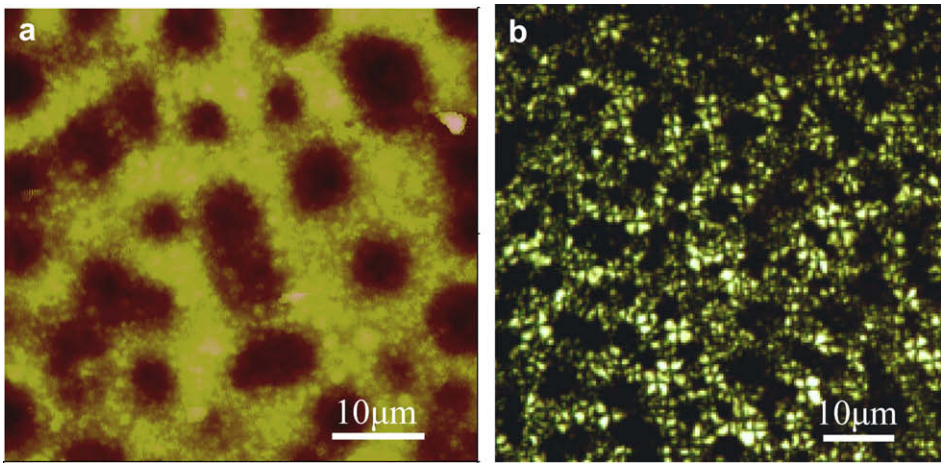

Fig. 10. AFM (a) and PLM (b) images of a blend of 70/30 HDPE/LLDPE crystallized at 120 °C after isothermal annealing at 170 °C for 24 h. (a) The nucleation-limited mechanism with spherical phase morphology, indicating that the phase separation occurs in between the binodal and spinodal curves; (b) the HDPE spherulites grow outside of the spherical phase domains.

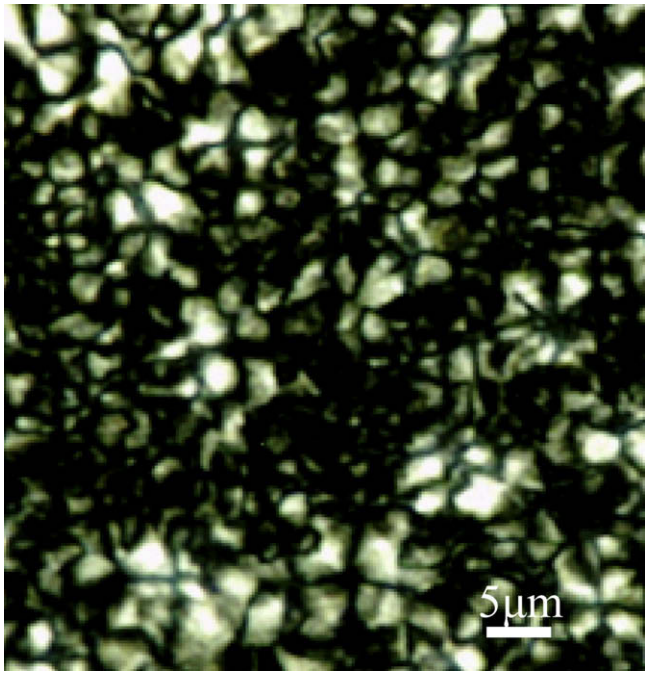

Fig. 11. PLM image of a blend of 70/30 HDPE/LLDPE crystallized at 120 °C after isothermal annealing at 155 °C for 24 h. The spinodal decomposition mechanism generates a bicontinuous phase morphology, indicating that the phase separation occurs below the spinodal curve. The HDPE spherulites grow within one of the bicontinuous phase domains.

theory. It is shown as the dotted line in Fig. 12. The calculated spinodal curve is a close approximation to the projected line from the experimental data points. From the calculation, it was determined that the critical HDPE composition is 48%, and the critical temperature is 187 °C. The critical value of the interaction parameter is 3.49×10^{-4}, which matches the value estimated for this type of blend [41–43]. By neglecting composition and molecular weight effects, we can simply adopt the interaction parameter form: $\chi = A/T + B$. Here, the interaction parameter is only a function of temperature. Experimental data fitting indicates that $\chi = 0.2735/T - 2.4454 \times 10^{-4}$.

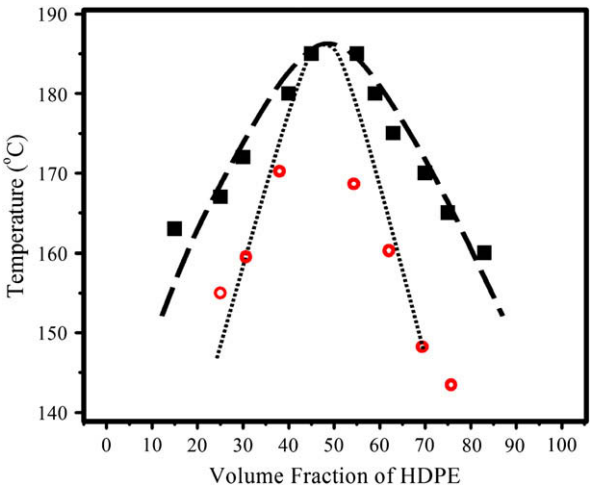

Fig. 12. Complete phase diagram for this series of HDPE/LLDPE blends. The binodal curve is determined by the onset of a decrease in the $t_{1/2}$ values (increase of the overall crystallization rates) as shown in Fig. 6, while the spinodal curve is determined by the phase morphology change. The dotted line is a Flory–Huggins prediction of the spinodal line.

Finally, this approach still needs to be accepted with care. In a real system, the spinodal line only exists in a perfect "mean-field" blend. In reality, this line can be alternately described as a temperature region. Therefore, we speculate that we should see a region in which the phase morphological change is gradual. Further detailed experiments need to be conducted to explore this aspect.

4. Conclusion

A newly designed two-step isothermal experiment provides an effective way to experimentally monitor liquid–liquid phase separation of PE blends. For binary blends with a crystallizable component and an amorphous component with isorefractive indices, such as in the case of this series of HDPE/LLDPE blend, the binodal curve can be estimated from the enhancement of crystallization rates. This estimation is close to the thermodynamic binodal curve. In addition, the spinodal curve can be determined from the spherulitic crystal decoration of the phase morphology. The theoretical calculations support the spinodal curve deduced from the morphological changes. This two-step isothermal experimental approach overcomes the difficulty in determining the miscibility of isorefractive index crystalline–amorphous blends and provides a way to determine the spinodal curve for liquid–liquid phase separation in those polymer blends.

Acknowledgments

This work was supported by the National Science Foundation (DMR-0516602) and a graduate fellowship provided by the Chevron-Phillips Chemical Company. In Peking University, the research was supported by the Chinese 973 Project (2003CB15605). The samples were provided by Dr. Manika Varma-Nair at Exxon Mobil Engineering Company. We also acknowledge Perkin–Elmer Co. for their support in providing a Diamond DSC instrument for our laboratory.

References

[1] Chun SP, Kao CL, Knight GW. Structure, properties and preparation of polyolefins produced by single-site catalyst technology. In: Schiers J, Kaminsky W, editors. Metalocene-based polyolefins: preparation, properties and technology, vol. 1. New York: Wiley and Sons; 2001. p. 261.
[2] Sinn H, Kaminsky W. Adv Organomet Chem 1980;18:99–149.
[3] Malmberg A, Kokko E, Lehmus P, Löfgren B, Seppälä JV. Macromolecules 1998;31:8448–54.
[4] Lohse DJ. Polyolefins. In: Craver CD, Carraher Jr CE, editors. Applied polymer science: 21st century. New York: Elsevier; 2000. p. 73.
[5] Paul DR, Bucknall CB, editors. Polymer blends. New York: John Wiley and Sons; 2000.
[6] Utracki LA, editor. Polymer blends handbook. Dordrecht/Boston/London: Kluwer Academic Publishers; 2002. p. 203.
[7] Kresge EN. In: Paul DR, Newman A, editors. Polymer blends, vol. 2. New York: Academic Press; 1978. p. 292.
[8] Nicholson JC, Finerman TM, Crist B. Polymer 1990;31:2287–93.
[9] Alamo RG, Londono JD, Mandelkern L, Stehling FC, Wignall GD. Macromolecules 1994;27:411–7.
[10] Wignall GD, Londono JD, Lin JS, Alamo RG, Galante MJ, Mandelkern L. Macromolecules 1995;28:3156–67.
[11] Alamo RG, Graessley WW, Krishnamoorti R, Lohse DJ, Mandelkern L, Stehling FC, et al. Macromolecules 1997;30:561–6.
[12] Wignall GD, Alamo RG, Londono JD, Mandelkern L, Kim MH, Lin JS, et al. Macromolecules 2000;33:551–61.
[13] Hill MJ, Barham PJ, Keller A. Polymer 1991;32:1384–93.
[14] Hill MJ, Barham PJ, Keller A. Polymer 1992;33:2530–41.
[15] Hill MJ, Barham PJ, Ruiten JV. Polymer 1993;34:2975–80.
[16] Hill MJ, Barham PJ. Polymer 1995;36:1523–30.
[17] Morgan RL, Hill MJ, Barham PJ. Polymer 1999;40:337–48.
[18] Kammer HW. Polymer 1999;40:5793–7.
[19] Crist B, Hill MJ. J Polym Sci Polym Phys 1997;35:2329–53.
[20] Wang H, Shimizu K, Hobbie EK, Wang ZG, Meredith JC, Arim A, et al. Macromolecules 2002;35:1072–8.
[21] Wang H, Shimizu K, Kim H, Hobbie EK, Wang ZG, Han CC. J Chem Phys 2002; 116:7311–5.

[22] Zhang XH, Wang ZG, Dong X, Wang DJ, Han CC. J Chem Phys 2006;125:024907.
[23] Tanaka H, Nishi T. Phys Rev Lett 1985;55:1102–5.
[24] Tanaka H, Nishi T. Phys Rev A 1989;39:783–94.
[25] Keller A, Cheng SZD. Polymer 1998;39:4461–87.
[26] Cheng SZD, Keller A. Annu Rev Mater Sci 1998;28:533–63.
[27] Cheng SZD. Phase transitions in polymers: the role of metastable states. Amsterdam: Elsevier; 2008. p. 266.
[28] Fu Q, Chiu F-C, McCreight KW, Guo M, Tseng WW, Cheng SZD, et al. J Macromol Sci Phys 1997;B36:41–60.
[29] Chiu F-C, Wang Q, Fu Q, Honigfort PS, Cheng SZD, Hsiao BS, et al. J Macromol Sci Phys 2000;B39:317–31.
[30] Wunderlich B. Macromolecular physics, vol. 1. New York/London: Academic Press; 1973. p. 388.
[31] Cheng SZD, Wunderlich B. J Polym Sci Polym Phys 1986;24:577–94.
[32] Cheng SZD, Wunderlich B. J Polym Sci Polym Phys 1986;24:595–617.
[33] Cheng SZD, Bu H-S, Wunderlich B. J Polym Sci Polym Phys 1988;27:1947–64.
[34] Alfonso GC, Russell TP. Macromolecules 1986;19:1143–52.
[35] Di Lorenzo ML. Prog Polym Sci 2003;28:663–89.
[36] Mareau VH, Prud'homme RE. Macromolecules 2003;36:675–84.
[37] Hunag P, Zhu L, Guo Y, Ge Q, Jing AJ, Chen WY, et al. Macromolecules 2004;37:3689–98.
[38] Takenaka M, Tanaka K, Hashimoto T. Mechanism and dynamics of ordering process of polymer blends at phase transition. In: Culberston WM, editor. Contemporary topics in polymer science, vol. 6. New York: Plenum Press; 1989. p. 363.
[39] Debenedetti PG. Metastable liquids: concept and principle. Princeton: Princeton University Press; 1996. p. 105, 199.
[40] Hashimoto T. Phase Transitions 1988;12:47–119.
[41] Londono JD, Narten AH, Wignall GD. Macromolecules 1994;27:2864–71.
[42] Graessley WW, Krishnamoorti R, Reichart GC, Balsara NP, Fetters LJ, Lohse DJ. Macromolecules 1995;28:1260–70.
[43] Schipp C, Hill MJ, Barham PJ, Clocke VM, Higgins JS, Oiarzabal L. Polymer 1996;37:2291–7.